Surface & Coatings Technology 446 (2022) 128772

Contents lists available at ScienceDirect

Surface & Coatings Technology

journal homepage: www.elsevier.com/locate/surfcoat

Solid lubricity of WS_2 and Bi_2S_3 coatings deposited by plasma spraying and air spraying

Philipp G. Grützmacher [a,*], Michael Schranz [a], Chia-Jui Hsu [a], Johannes Bernardi [c], Andreas Steiger-Thirsfeld [c], Lars Hensgen [d], Manel Rodríguez Ripoll [b], Carsten Gachot [a]

[a] Institute for Engineering Design and Product Development, Tribology Research Division, TU Wien, Lehárgasse 6–Objekt 7, 1060 Vienna, Austria
[b] AC2T research GmbH, Viktor-Kaplan-Straße 2/C, 2700 Wiener Neustadt, Austria
[c] University Service Centre for Transmission Electron Microscopy (USTEM), TU Wien, Wiedner Hauptstraße 8-10, 1040 Vienna, Austria
[d] Tribotecc GmbH, Industriestraße 23, 9061 Arnoldstein, Austria

ARTICLE INFO

Keywords:
2D layered materials
Solid lubricant coatings
Deposition process
Plasma spraying
Air spraying

ABSTRACT

Lubrication is highly relevant for the reliability and longevity of any moving machinery. Machines are mainly lubricated by oils or greases but there are many conditions especially for low and high temperature applications, under vacuum or for hygienic reasons where conventional oil and grease lubrication cannot be applied. Under these circumstances, solid lubricants such as those based on layered materials (MoS_2, WS_2 or Bi_2S_3) are the right choice to maintain a safe and reliable operation of machines. However, the tribological performance of the solid lubricant does not only depend on the chemical composition but also the deposition technique used. In this research article, we deposited coatings of WS_2 and Bi_2S_3 by atmospheric plasma spraying and a simple air spray coating process. The friction and wear behaviour was studied at three different temperatures: room temperature, 100 °C, and 200 °C. To gain insight into the acting lubrication mechanisms, the morphological and chemical properties of the resulting wear tracks were investigated by light microscopy and Raman spectroscopy. It was demonstrated that atmospheric plasma spraying leads to a thermal decomposition of the feedstock powders and is therefore not recommendable as deposition technique. In contrast, simple air spraying results in well-performing solid lubricant coatings with superior friction and wear properties for WS_2 compared to Bi_2S_3 even at an elevated temperature of 200 °C.

1. Introduction

Solid lubricants are used in many applications where the use of liquid lubricants is simply limited. Two prominent examples are space applications and metal processing, where vacuum or high temperatures prevail [1,2]. Solid lubricants can be classified into seven classes according to their lubrication mechanisms: (i) soft metals (e.g., tin or gold); (ii) fluorides (e.g., LiF, CaF_2); (iii) polymers (e.g., PTFE); (iv) hard carbon-based materials such as diamond-like carbon (DLC); (v) binary and ternary oxides; (vi) easy to shear bulk materials such as MAX phases; and (vii) two-dimensional (2D) layered materials like MXenes or transition metal dichalcogenides (TMDs) [3–5].

The first 2D layered materials used for friction reduction were TMDs (MS_2 and MSe_2 with M = Mo or W). TMDs are characterized by transition metal atoms sandwiched between two layers of chalcogen atoms forming a S–M–S molecular layer. The low shear between molecular layers provides them with excellent frictional properties [6]. Later, the popularity of 2D layered materials significantly rose after the successful mechanical exfoliation of graphene in 2004 [7–9]. Other 2D materials, which have shown interesting tribological properties are black phosphorous [10], hexagonal boron nitride (h-BN) [11], and MXene [12,13]. Their outstanding potential to serve as solid lubricants can be traced back to the strong in-plane bonds giving them extreme strength, but only weak out-of-plane coupling between adjacent layers resulting in easy sliding of individual layers over each other [8,14]. Given the right circumstance even superlubricity (i.e., coefficient of friction (COF) < 0.01) can be achieved with 2D materials [15]. Additionally, the outstanding mechanical properties of these materials result in very high wear resistance [8].

One of the most studied and applied solid lubricants is the TMD MoS_2, which is particularly interesting for space applications due to its reliable lubrication properties in vacuum and at low temperatures [16].

* Corresponding author.
E-mail address: philipp.gruetzmacher@tuwien.ac.at (P.G. Grützmacher).

https://doi.org/10.1016/j.surfcoat.2022.128772
Received 13 April 2022; Received in revised form 26 July 2022; Accepted 2 August 2022
Available online 8 August 2022

For terrestrial or high temperature applications, however, MoS_2 is not well suited because of the rapid loss of lubricity and accompanied high wear under these conditions [16]. Therefore, for such applications, other materials have to be applied. Two other layered sulphides, which perform better in these environments are WS_2 and Bi_2S_3 [17,18]. Both materials can be used as additives in base oils and are reported to form layered tribofilms, thus effectively reducing friction and wear [18,19]. For applications at higher temperature, the use of solid lubricants in the form of coatings is preferable.

Despite demonstrating high potential for friction and wear reduction, wear life is often a problem encountered when 2D solid lubricant coatings are used [20]. In this context, adhesion between coating and substrate is critical, which is influenced by the coating technique [21]. Solid lubricant coatings can be applied by a wide variety of coating techniques [22], starting from relatively simple techniques like drop-casting [23] or spray coating deposition [24], burnishing [25], thermal spraying [26], electrophoretic deposition (EPD) [27], physical vapor deposition (PVD) techniques [28] to chemical vapor- (CVD) [29] and atomic layer deposition (ALD) [30]. For a successful coating process, the surface geometry of the substrate, the environmental conditions during the coating process, achievable coating thicknesses, applicability to the coating material, and the complexity of the process have to be taken into consideration [31]. Thermal spraying techniques are able to form dense and wear resistant coatings with high adhesion to the substrates [32,33]. This makes them attractive as coating technique in several industry sectors like aerospace, biomedical, and automotive [33]. Chen et al. used atmospheric plasma spraying to generate nanostructured zirconia coatings and demonstrated high wear resistance during sliding at loads between 20 and 80 N [34]. A disadvantage of plasma-sprayed coatings are the high temperatures of up to 25,000 °C occurring locally, which might lead to the decomposition of the sprayed powder [35]. A mild and quite simple technique to deposit solid lubricant coatings is spray coating [31,36], where the solid lubricant particles simply have to be dispersed in a suitable solvent and then sprayed onto the substrate using pressurized gas.

Despite the great effect of the coating technique on the tribological performance of layered sulphide particles, investigations on this aspect are scarce. Therefore, we investigated the tribological properties of WS_2 and Bi_2S_3 coatings deposited by an atmospheric plasma spray (APS) process and a relatively simple spray coating (SC) technique, motivated by the need for a coating technique able to generate high performing coatings for tribological applications. The tribological tests were performed from room temperature up to 200 °C to test the performance of the coatings even at slightly elevated temperatures. The tribochemical reactions occurring in the contact zone during sliding were analysed by Raman spectroscopy.

2. Materials and methods

2.1. Substrate and solid lubricant powder

AISI304 steel discs with a diameter of 25 mm, a thickness of 5 mm, and a S_q roughness of 0.65 μm were used as substrate for the coatings and the subsequent tribological tests. The feedstock powder for the coatings were WS_2 and Bi_2S_3 (Tribotecc, Austria) with a purity of 98.5 %. Table 1 lists the densities and particle size distributions of the powders.

Table 1
Powder characteristics of the WS_2 and Bi_2S_3 powders used as starting material.

Parameter	WS_2	Bi_2S_3
Density (g/cm^3)	7.7	6.9
Particle size distribution d50 (μm)	7.0	18
Particle size distribution d90 (μm)	14.0	41

2.2. Atmospheric plasma spraying

One set of samples was coated by atmospheric plasma spraying (INOCON Technologie GmbH, Austria). Before the coating process the samples were cleaned using acetone in an ultrasonic bath for 10 min. The samples were attached onto a plane table and were coated in a single step for a given powder type. To improve the feedability of the powder to the plasma spraying gun, 3 g of amorphous SiO_2 particles were added to 100 and 160 g of WS_2 and Bi_2S_3 powder, respectively. Argon was used as processing gas, which was ionized in the plasma gun resulting in an expansion of the gas and an acceleration of the powder added to the plasma inside the gun towards the substrate surface. The gun was positioned over the samples at a distance of 50 mm by an industrial robot and the deposition process was performed following parallel deposition tracks with a distance between individual scanning lines of 3 mm. The process parameters are listed in Table 2.

2.3. Spray coating

Spray coating with an airbrush gun was performed as a simple alternative to plasma spraying. After evaluating several solvents, ethanol was chosen as it gave the most stable dispersions. The powders were added to 100 ml ethanol with a concentration of 0.25 wt.-%. To improve the dispersibility and to reduce agglomeration of the powder particles the dispersions were treated in ultrasonic bath for 10 min. Directly after ultrasonication, the dispersion was transferred to the solvent container of the airbrush gun (Timbertech). The airbrush gun was connected to a compressor operating at an air pressure of 2 bar. The dispersed particles were accelerated in the air flow onto the samples, heated to a temperature of 100 °C by a heating table (Fisherbrand). The working distance between nozzle and sample was set to 12 cm. For each sample a dispersion volume of 40 ml was used.

2.4. Tribological experiments

The tribological experiments were performed on a SRV4 tribometer (Optimol Instruments) in linear reciprocating sliding mode under dry contact conditions without any additional lubrication. 100Cr6 steel balls with a diameter of 10 mm were used as counterbody. The stroke length was 1.0 mm and the frequency 5 Hz, resulting in a sliding speed of 2 mm/s. The load was kept constant for all tests at 5 N, giving a Hertzian contact pressure of 786 MPa for the uncoated sample. To study the effect of temperature on the tribological behaviour of the solid lubricant coatings the tests were performed at room temperature, 100 °C, and 200 °C. Short term tests were performed with a duration of 900 s, whereas long term tests had a duration of 40 min.

2.5. Materials characterisation

The surface topography of the samples was imaged by laser scanning microscopy (LSM, VK-X1100, Keyence) and by scanning electron microscopy (SEM, XL 30, FEI Philips) before and after the coating process as well as after the tribological experiments. Cross-sections through the coatings were prepared by focused ion beam (FIB) in the SEM.

The chemical composition of the powders and the coatings (before and after the tribological experiments) was characterized by Raman

Table 2
Process parameters for the atmospheric plasma spraying process.

Parameter	WS_2	Bi_2S_3
Current (A)	140	140
Scanning velocity (mm/s)	50	250
Powder feeding rate (g/min)	2.0–2.5	3.0
Number of coating steps	6	1
Scanning distance (mm)	50	50

spectroscopy and X-ray diffraction (XRD). For the Raman analysis, a Raman spectrometer (HR800, Jobin Yvon Horiba) with a wavelength of 532 nm and a yielded laser power of 13.5 mW was used. The spot size was 20 μm and the measuring time 3 s. XRD analysis was performed on a PANalytical Empyrean system using 45 kV and 40 mA with Cu Kα irradiation.

The adhesion of the coatings was determined using a scratch tester (Millennium 100, TRIBOtechnic) using a standard Rockwell-C diamond cone with an angle of 120° and a tip radius of 200 μm. The scratch tests were performed with a linear increase in load from 1 to 30 N for a total scratch length of 10 mm, with a scratch velocity of 0.167 mm/s. After the experiments, the scratches were investigated using a scanning electron microscope (JEOL JIB-4700F, Jeol Ltd.) equipped with an energy dispersive X-ray spectroscopy (EDX) detector (Bruker XFlash 6|30, Bruker Corporation).

3. Results and discussion

3.1. Characterisation of solid lubricant coatings

WS_2 and Bi_2S_3 solid lubricant coatings were deposited on technologically relevant AISI 304 steel surfaces with a surface of 3.3 cm^2. The coatings were applied to the surfaces using two different coating techniques, namely atmospheric plasma spraying and air spraying to investigate the role of the deposition technique on the resulting coating quality and their tribological properties. SEM analyses in Fig. 1 show the feedstock powders and the surfaces after deposition of the WS_2 and Bi_2S_3 coatings. Irrespectively of the applied coating technique, the solid lubricant particles are homogeneously distributed on the sample surface. In case of plasma sprayed coatings, the flake-like structure of the initial particles cannot be observed after deposition, which can be traced back to partial melting of the particles induced by the extreme temperatures of up to 25,000 °C reached during the deposition process [32]. Resolidified material can also be clearly seen on the surfaces coated by plasma spraying. The partial melting of the material, also leading to a reduction in particle size, is particularly pronounced for the smaller WS_2 particles, whereas the larger Bi_2S_3 particles are still partially visible on the surface. The higher melting point of the WS_2 particles (1250 °C for WS_2 vs 765 °C for Bi_2S_3, according to the supplier's data sheets) seems to only play a subordinate role at these high temperatures, which greatly exceed the melting temperature of both particle types. On the contrary, the initial particle size is the decisive factor in terms of the coatings' morphology. The larger Bi_2S_3 particles only allow for a partial melting of the particles' surface in the short time where high temperatures prevail. Therefore, the plasma sprayed Bi_2S_3 coatings are characterized by larger particle agglomerates as well as higher roughness, and porosity. The melting of the particles in combination with the high impact velocities of the powder particles results in a complete coverage of the sample surface

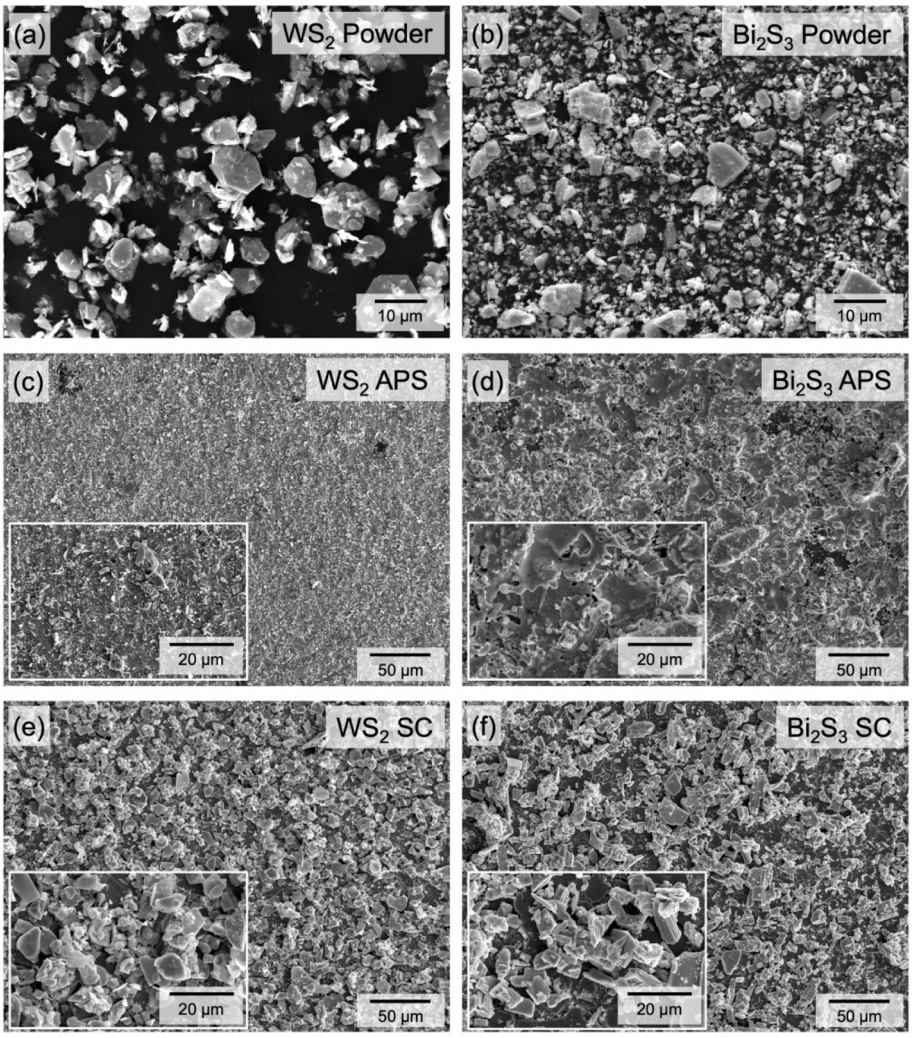

Fig. 1. Scanning electron microscopy (SEM) images of the (a,b) feedstock WS_2 and Bi_2S_3 powders and the coatings deposited by (c,d) atmospheric plasma spraying (APS) and (e,f) spray coating (SC). The insets show SEM micrographs at higher magnification.

with a rather dense coating. On the other hand, the initial flake-like morphology of the particles is still clearly visible for the coatings deposited by spray coating. As a result of the stochastic nature of the spray coating process and due to the lower density of the coating since the solid lubricant powder is not melted, the substrate surface is still partially visible at some locations. This is more pronounced in case of the Bi_2S_3 coatings due to the larger particle size. The roughness of the samples is significantly increased after depositing the coatings from an initial value of 0.65 µm (S_q) to 0.95 µm and 3.73 µm for the WS_2 and Bi_2S_3 plasma sprayed and to 2.37 µm and 3.86 µm for the WS_2 and Bi_2S_3 spray coated samples, respectively. The comparatively lower S_q value for the plasma sprayed WS_2 coating indicates again a significant melting of the particles during the deposition process, whereas in case of Bi_2S_3, some of the larger particles are only partially molten at their outer surface. The stochastic nature of the air spray coating deposition technique and the anisotropy of the particle shape results in a high roughness for both particle types, while the Bi_2S_3 coating is again even rougher due to a larger particle size of the feedstock powder.

A more detailed view of the deposited coating thickness and morphology is provided by means of FIB cross-sections through the respective coatings, as depicted in Fig. 2. All coatings have a coating thickness in the lower µm range, despite varying between roughly 1.0 and 5.0 µm. The plasma sprayed coatings are very homogeneous in terms of their thickness, whereas the coating thickness of the spray coated samples varies substantially as result of the stochastic nature of the process. The lowest coating thickness is measured for the plasma sprayed WS_2 sample (Fig. 2a), which is a result of the small initial particle size and the pronounced melting of the particles leading to a dense but thin coating. In contrast, the resulting thickness of the plasma sprayed Bi_2S_3 coating is higher with several pores and cracks visible throughout the cross-section (Fig. 2b). Again, the increased thickness is due to the larger initial particles, which are not completely melted during the process, thus leading to a thicker and porous coating despite the smaller amount of material processed. The cracks on the surface of the Bi_2S_3 coating are likely a result of high thermal and mechanical stresses at the impact of the droplets on the substrate surface. In the insets showing higher magnifications of the coatings, it can be well observed how the molten material, generated during the plasma spraying process, is flowing into the surface roughness (Fig. 2a and b). This leads to a mechanical interlocking of the material onto the surface, which is responsible for the excellent adhesion of plasma sprayed coatings [37]. The significant difference of the coatings' morphology is verified by analysing the cross-sections of the coatings deposited by spray coating. While the layered morphology of the particles is mostly lost during the plasma spraying process, individual platelets are present in the spray-coated samples (Fig. 2c and d). Here the larger size of the Bi_2S_3 particles, particularly in terms of particle thickness, can unambiguously be seen. The WS_2 platelets exhibit a thickness of <1 µm, while the Bi_2S_3 particles are up to 2 µm thick. Additionally, it seems as if the thinner WS_2 particles are preferentially aligned parallel to the substrate, whereas some of the thicker Bi_2S_3 particles are almost oriented vertically.

The phase compositions of the coatings after the deposition process were measured using XRD analysis. The feedstock powders indicate a high purity, with elemental tungsten and bismuth being present as impurities (Fig. 3). Comparing the XRD spectra of the initial powders with the ones obtained after the respective coating processes demonstrates the increased occurrence of elemental tungsten and bismuth after the plasma spraying process, leading to a concentration of up to 70 wt% and 50 wt% (obtained from relative peak intensities) of elemental tungsten and bismuth, respectively. This can be traced back to the extremely high temperatures reached during the deposition process, at which the decomposition of WS_2 and Bi_2S_3 particles takes place. For the plasma sprayed WS_2 coatings some mild oxidation of tungsten into WO_3 is also indicated. In contrast, the spray coating process does not result in a phase change of the powder, which is not surprising considering the mild conditions prevailing during deposition).

The adhesion of the deposited coatings was investigated via scratch tests. The results in Fig. 4 unambiguously demonstrate the higher adhesion of the plasma sprayed coatings compared to the spray coated samples. For both plasma sprayed coatings, some dark patches are visible after 1 or 2 mm scratching, which corresponds to coating delamination and exposure of the substrate material. This is in accordance with the energy dispersive X-ray spectroscopy (EDX)

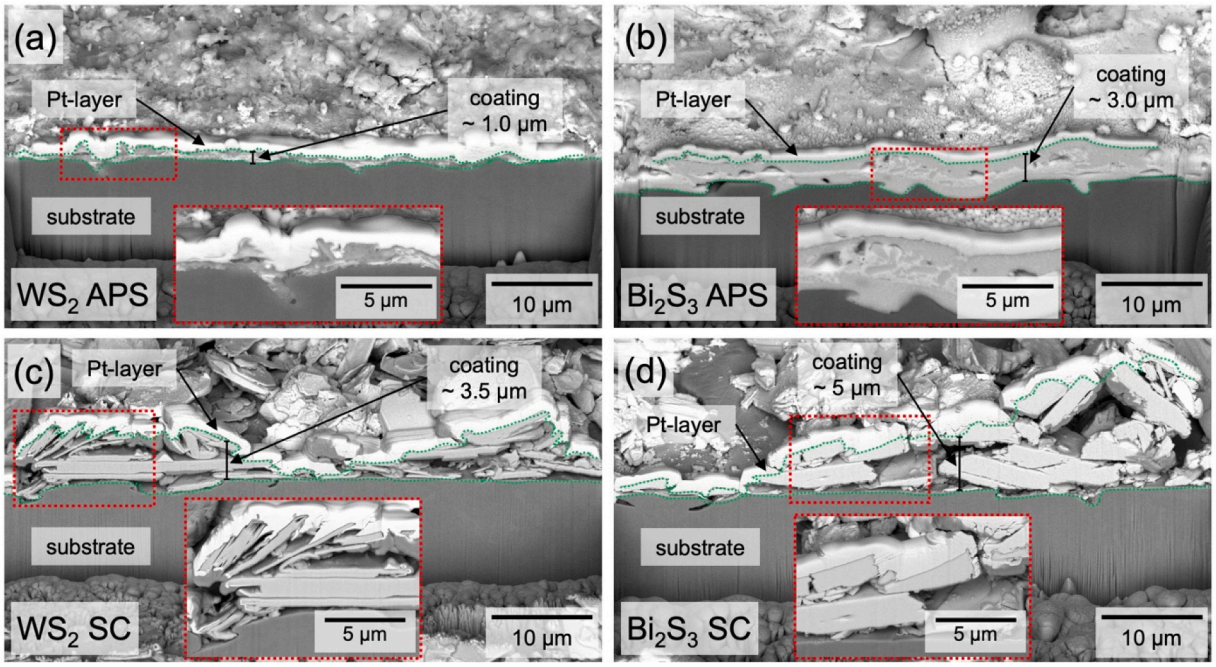

Fig. 2. Cross-sections of the prepared coatings by focused ion beam (FIB). The top images show the (a) WS_2 and (b) Bi_2S_3 coatings prepared by atmospheric plasma spraying and the bottom images the (c) WS_2 and (d) Bi_2S_3 coatings prepared by spray coating. For each cross-section, a higher magnification micrograph of the coating is provided. The coatings are marked with a green dashed line and an estimation of the coating thickness is given.

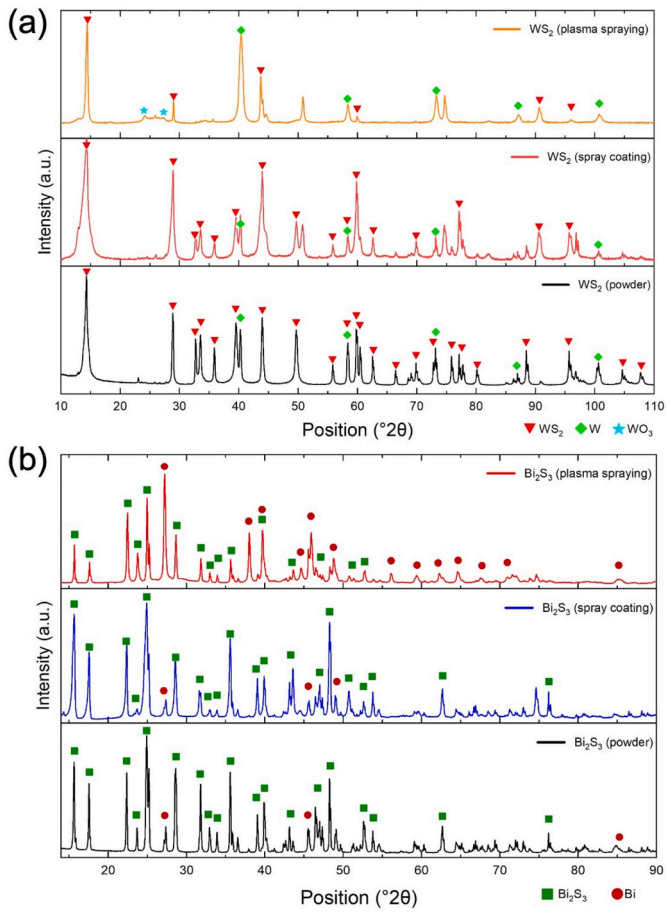

Fig. 3. XRD analysis of the (a) WS_2 and (b) Bi_2S_3 feedstock powders before the deposition process and the coatings prepared by atmospheric plasma spraying and spray coating.

measurements showing a similar reduction in the content of W and Bi over the length of the scratch. On contrary, the adhesion of the spray coatings to the substrate is much lower. In particular, the WS_2 spray coating seems to be completely removed right at the onset of the scratch experiment. The spray coated Bi_2S_3 sample demonstrates slightly higher adhesion, but was also removed much faster when compared to its plasma spray counterpart.

3.2. Tribological characterisation

To study the tribological performance of WS_2 and Bi_2S_3 coatings as a function of the deposition technique, i.e., plasma spraying or spray coating, ball-on-disk tests were carried out at room temperature, 100 °C, and 200 °C. The results of the measurements at room temperature are presented in Fig. 5. The uncoated substrates show the typical behaviour of a dry, non-lubricated steel-steel pairing under sliding contact. The COF starts at around 0.3 and then quickly rises to its steady state value of around 0.95 within the first 200 s, which can be associated with the flattening of asperities and the corresponding increase of the real contact area as well as the removal of thin oxide layers and contaminants, leading to higher adhesion and, finally, higher friction [38].

All coated samples start at a slightly lower COF of around 0.2. However, both samples coated by the plasma spraying technique show a rapid increase in friction. The plasma sprayed WS_2 sample shows a stable COF of 0.2 for the first 50 s and then friction continuously increases until the COF reaches the steel-on-steel reference value after 300 s of sliding (Fig. 5a). The plasma sprayed Bi_2S_3 sample even displays a faster increase in friction with a jump to 0.5 in the very first stages of sliding from where the COF is continuously increasing until reaching the reference level after 400 s (Fig. 5b). Therefore, it can be concluded that the lubricious properties of the WS_2 and Bi_2S_3 particles are degraded following the plasma spraying process, leading to excessive wear rates and short coating lifetimes. The high friction of these coatings can be associated with the solid lubricant particles' partial decomposition from the sulphide phase into metallic bismuth or tungsten during the process and the accompanying loss of their layered structure, which is the basis for their low friction lubrication mechanism [17,39]. This will be later on verified by characterisation of the resulting wear tracks and Raman analysis. The lower concentration of lubricious sulphides also results in a lower availability of lubricious particles in the contact zone, which

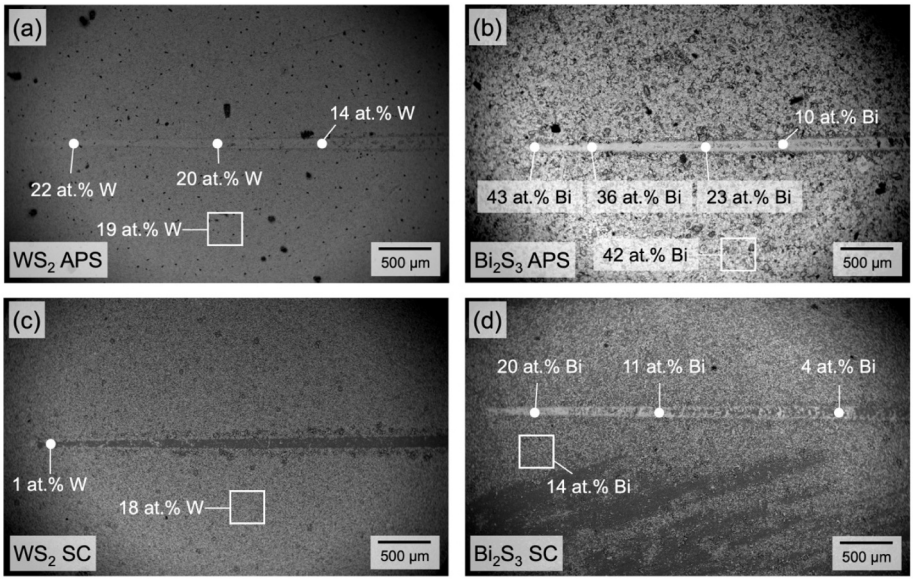

Fig. 4. Scratch tests of the prepared coatings. The top images show the initial 3 mm of the scratch tests on the (a) WS_2 and (b) Bi_2S_3 coatings prepared by atmospheric plasma spraying and the bottom images the scratch tests on the (c) WS_2 and (d) Bi_2S_3 coatings prepared by spray coating. The elemental composition of the scratch was measured at predefined positions using energy dispersive X-ray spectroscopy (EDX).

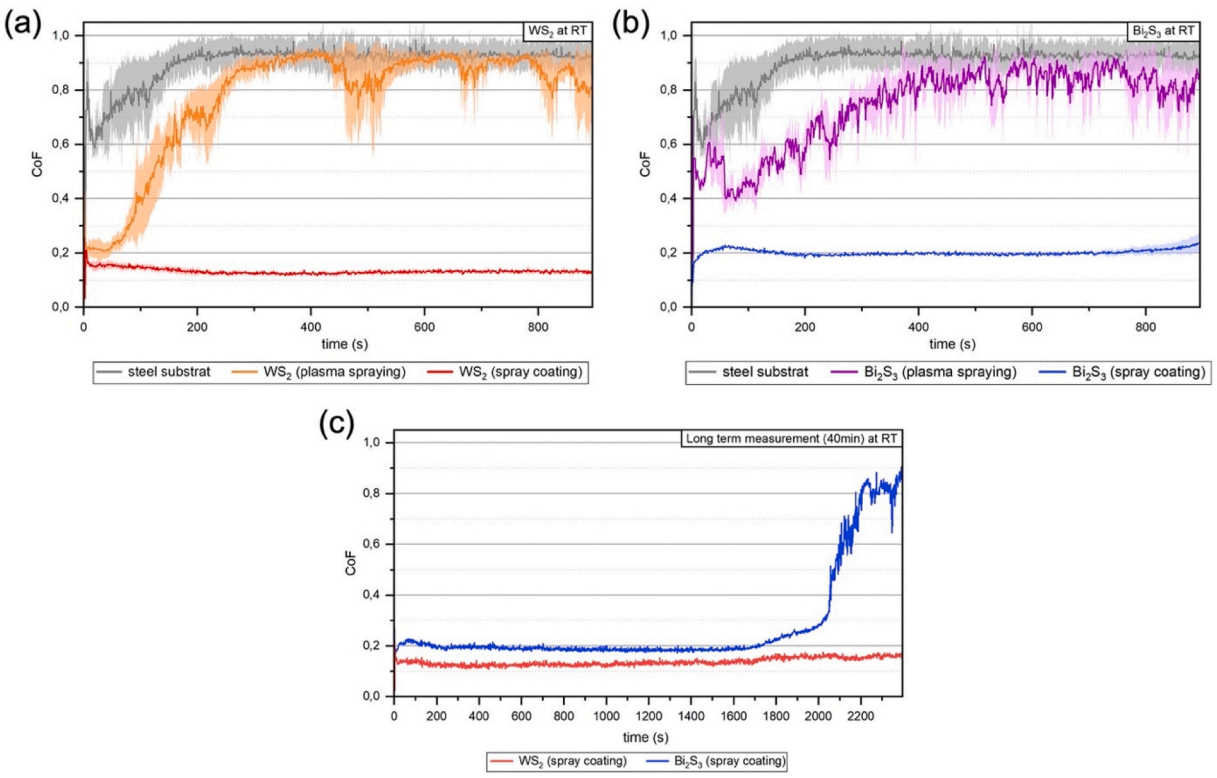

Fig. 5. Evolution of the COF of the uncoated reference sample and the samples coated with (a) WS2 particles and (b) Bi_2S_3 particles by both plasma spraying and spray coating at room temperature over a period of 900 s. Additionally, the (c) long term measurements of the spray coated samples at room temperature are presented.

negatively affects the wear life of the coatings. Moreover, the high prevailing friction generally results in a fast removal of the coatings from the contact zone. Both these factors lead to substantially lower wear life and, after a short running-in phase the same frictional behaviour as the uncoated reference.

On the contrary, the spray coated samples demonstrate a stable low steady-state friction in the short sliding experiments up to 900 s. After a brief running-in phase, in which the COF of the spray coated WS_2 sample drops from 0.20 to 0.12, its value remains stable at 0.13 throughout the experiment (Fig. 5a). It is noteworthy that the standard deviation of the measured COF values is rather low, reflecting an excellent repeatability of the experiments. The COF of the spray coated Bi_2S_3 sample slightly increases during running-in, and then stabilizes at a value of 0.20 until 800 s, when the COF and its standard deviation increase slightly (Fig. 5b). The reason for this behaviour is that at this point, one of the three measurements showed an increase in friction, which could be a first sign of failure of the deposited coating. This behaviour was confirmed in long-term experiments performed until 2400 s (40 min). Here, the spray coated Bi_2S_3 sample shows a stable COF of 0.20 until 1700 s of sliding, after which the COF slowly increases until a sharp rise in the COF occurs at 2000 s, indicating failure of the solid lubricant coating (Fig. 5c). The excellent performance of the spray coated WS_2 sample, on the other hand, is confirmed in the long-term tests, as the sample displayed a low and stable COF well below 0.20 until the end of the experiment at 2400 s. The low friction of the coatings fabricated by spray coating can be traced back to the lubrication mechanism of the two-dimensional WS_2 and Bi_2S_3 particles based on the low shear between individual layers and the formation of a protecting tribofilm, as highlighted in the next sections. Hence, it can be concluded that solid lubricant coatings of WS_2 and Bi_2S_3 with a layered structure deposited by a simple spray coating process facilitate beneficial tribological properties.

The tribological properties of the coated samples at elevated temperatures was tested at 100 °C for the plasma sprayed samples and at 200 °C for the spray coated samples (Figs. 6 and 7). The plasma sprayed samples demonstrate very similar frictional behaviour as for the measurements at room temperature with a quickly rising COF to the reference level (Fig. 6). However, the increase in COF for both the reference and for the plasma sprayed WS_2 and Bi_2S_3 samples is somewhat slowed down, probably due to temperature-induced enhanced oxidation of the steel, leading to a longer running-in phase until steady-state values are reached. Therefore, it can be concluded that plasma sprayed WS_2 and Bi_2S_3 coatings are also not suitable for application at slightly elevated temperatures.

Since the spray coated samples demonstrated stable and low frictional properties at room temperature, tribological tests were also conducted at a higher temperature of 200 °C in order to evaluate their performance at a temperature beyond the application range of many conventional liquid lubricants [40]. At this temperature the uncoated reference demonstrates a reduction in the COF over the first 50 s to 0.60, from where it increases again to reach its steady-state value of 0.80 after about 100 s (Fig. 7). The slightly lower steady-state value at this temperature compared to the room temperature measurements has also been reported in literature for steel-steel contacts [41,42] and can be correlated with the formation of a compacted debris bed of oxidized wear particles. As the oxidation rate at this temperature is faster, steady state conditions are reached slightly quicker compared to the measurements at room temperature. The WS_2 spray coated samples again clearly reveal an excellent frictional performance with a COF starting at 0.10, which then rises during the first 300 s of sliding to 0.19 from where it decreases again to a final value of 0.13 after 900 s of sliding (Fig. 7a). Therefore, the well-known high temperature lubricity of WS_2 particles can be verified for the samples prepared by using an inexpensive and simple spray coating process [43]. On the other hand, the COF of the samples spray coated with Bi_2S_3 particles starts already at a relatively high value of 0.40 from where it increases continuously until reaching

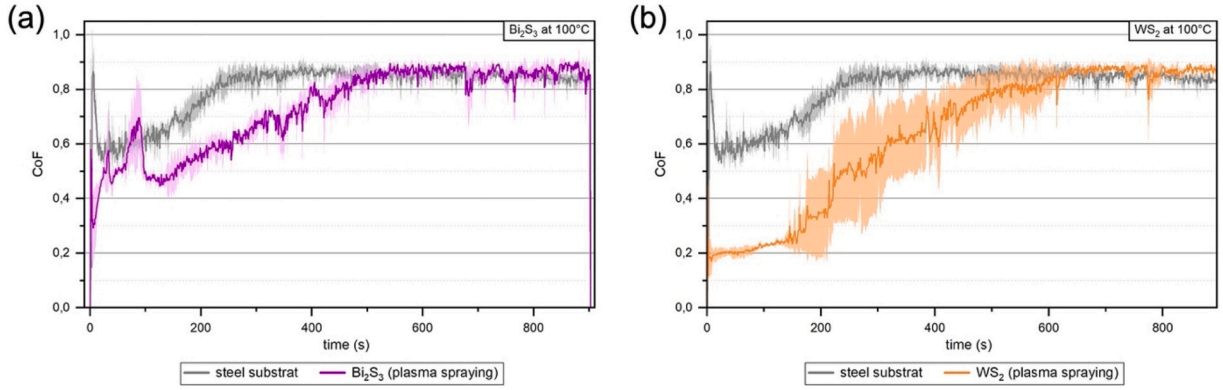

Fig. 6. Evolution of the COF of the uncoated reference sample and the samples coated with (a) WS_2 particles and (b) Bi_2S_3 particles by plasma spraying at 100 °C during 900 s.

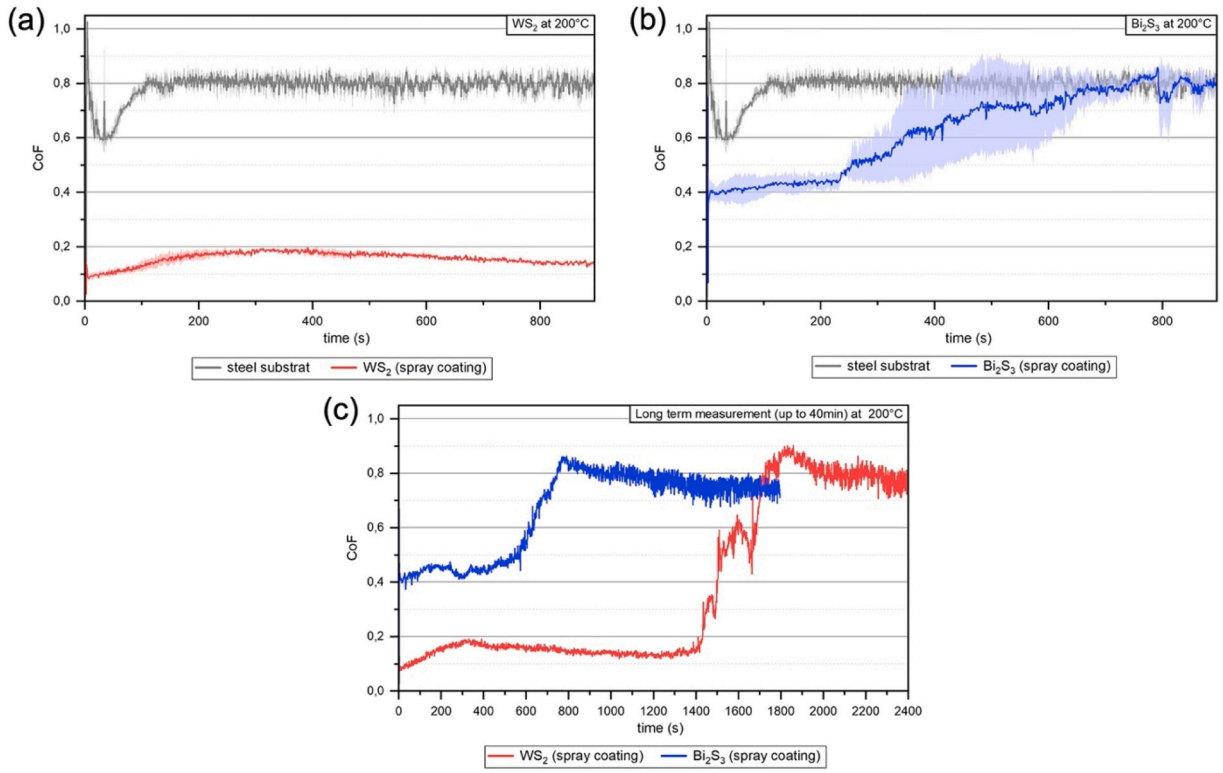

Fig. 7. Evolution of the COF of the uncoated reference sample and the samples coated with (a) WS2 particles and (b) Bi_2S_3 particles by both spray coating at 200 °C over a period of 900 s. Additionally, (c) long term measurements at 200 °C are presented.

the reference value of 0.80 after 700 s of sliding, which indicates failure of the coating (Fig. 7b). The initial value of 0.40 is in good accordance with earlier measured values for Bi_2S_3 coatings [18], keeping in mind that in the mentioned study the tests were only run for 30 s. For even higher temperatures above 500 °C, Bi_2S_3 might be a better choice, as it has been demonstrated to oxidize partially at these temperatures, forming bismuth oxysulfate [$Bi_{28}O_{32}(SO_4)_{10}$], which resulted in a significant reduction in friction [18]. These temperature ranges are, however, beyond the scope of the present study. Long term measurements up to 2400 s of the spray coated samples verify the excellent frictional performance of the respective coatings (Fig. 7c). While the Bi_2S_3 coating fails after 600 s of sliding, the COF of the WS_2 coating steadily remains below 0.20 until failing after 1400 s of sliding, surpassing the lifetime of their Bi_2S_3 counterpart by over a factor of 2. The longer wear life of the WS_2 coatings compared to Bi_2S_3 coatings, irrespectively of the testing temperature, can be correlated with the lower friction of the WS_2 coatings, leading to smaller stresses on this coating and therefore a slower removal. Additionally, this behaviour might be related to the shape of the particles. The smaller and thinner WS_2 particles are more easily aligned parallelly to the substrate surface (see also Fig. 2c), where they strongly adhere and form a protective tribofilm. The thicker Bi_2S_3 particles (Fig. 2d) on the other hand are not forming a well adhering tribofilm and are easily removed from the contact interface, therefore leading to failure of the coating and a corresponding high COF. In accordance to this, a recent work noticed a lower adhesion at high contact pressures of Bi_2S_3 to 100Cr6 balls used as counterbody [44] and justified this observation using ab initio simulations that revealed Bi_2S_3 has a lower number of S bonds per surface unit when compared to MoS_2, even though both compounds have a very similar surface adhesion energy. The shape of the particles may also play a role, as Li et al.

demonstrated better adherence to the surface for smaller $MoSe_2$ particles, thus improving tribofilm formation and leading to a better friction and wear performance [45].

3.3. Morphology and chemical composition of the worn coatings

The morphology of the coatings and counteracting balls are analysed using light microscopy, while the chemical composition in the contact zone is monitored by Raman spectroscopy, in order to get a detailed insight of the governing lubrication mechanisms. The wear occurring after 900 s of sliding at room temperature is in good agreement with the previously discussed friction behaviour (Fig. 8). The reference sample shows substantial abrasive and adhesive wear on both substrate and counterbody which is typical for non-lubricated sliding. Additionally, tribochemical oxidation of the substrate can be observed. The severe oxidation of the surface during sliding is confirmed by Raman, and the spectrum obtained from the wear track presents the characteristic peaks for iron oxide (Fe_3O_4) at 249, 299, 412, 613, and 660 cm^{-1} [46]. The observed surface oxidation in the wear track can be related to the increase in contact temperature caused by sliding [47]. The plasma sprayed samples, both with WS_2 and Bi_2S_3 particles, also demonstrate severe abrasive, adhesive, and tribochemical wear, with wear scars being of the same size as for the reference sample. The brownish colour observed in the wear tracks is a hint of the presence of iron oxide species generated from direct metal to metal contact. This finding is again verified by Raman spectroscopy. After 900 s of sliding, only iron oxides can be identified on the wear scar, as in case of the reference surface. The observed wear behaviour and the Raman results of the plasma sprayed coatings verify their failure with a complete removal of the coating, leading to high friction and high wear. The similar contact conditions with a high amount of oxidic wear debris and a comparable contact area for the reference sample and the samples coated by plasma spraying explain the nearly identical frictional behaviour observed towards the end of the experiment, see Fig. 5. In contrast, wear for the spray coated systems is greatly reduced at room temperature. Additionally, despite a similar appearance in the light microscopy images with low magnification, showing a dark patchy wear track, the insets with higher magnification indicate the formation of a rather continuous tribofilm on the spray coated substrates. This is further verified by Raman spectroscopy of the spray coated substrates' wear tracks. Here peaks related to WS_2 at 351 and 417 cm^{-1} [48]), WO_3 at 705 and 810 cm^{-1} [49], and Bi_2S_3 at 260, 610, and 965^{-1} [50] can be found, which is similar to the

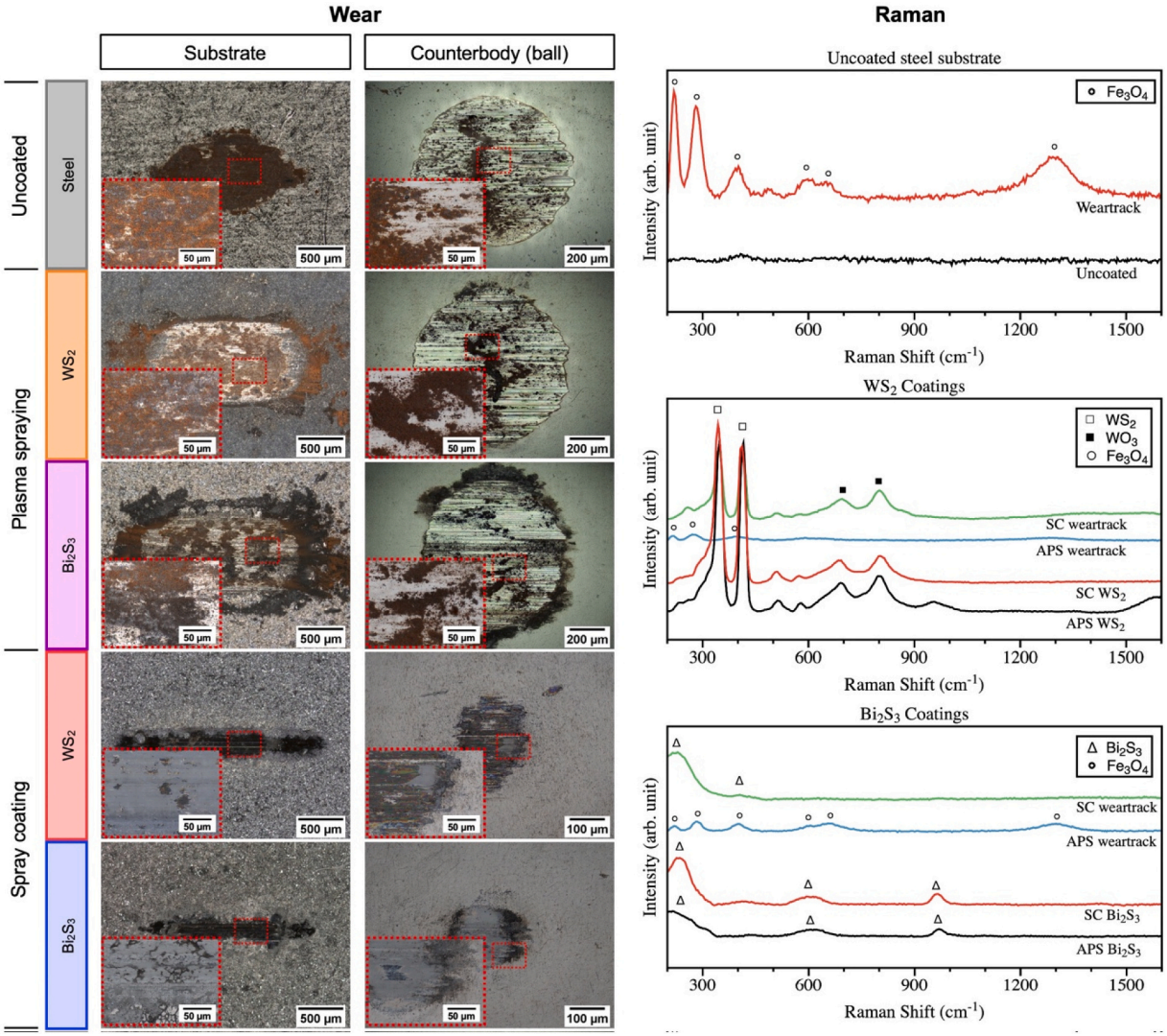

Fig. 8. Light microscopy images of the wear tracks on the substrates (left) and ball counterbodies (right) tested at room temperature for the uncoated reference sample as well as the coatings deposited by plasma spraying and spray coating with WS_2 and Bi_2S_3 particles. Magnified insets for individual wear track positions are shown for the regions highlighted with red rectangles. On the right-hand side, Raman spectra taken within the wear tracks on the WS_2 and Bi_2S_3 spray coated and plasma sprayed substrates measured at room temperature are shown.

situation before the tribological experiments. Conversely, no peaks related to iron oxide are measured. This proves the lack of degradation and full functionality of the WS_2 and Bi_2S_3 coatings fabricated by spray coating after tribological testing for 900 s at room temperature. Additionally, the black layer on top of the balls in the spray coated systems suggests the adhesive transfer of solid lubricant material to the ball surface and the formation of a tribofilm. Therefore, the spray coated samples measured at room temperature can successfully form a stable tribofilm/tribofilm system, protecting the surfaces and resulting in low shear and friction.

In case of the WS_2 spray coating, the presence of a fully functional and non-degraded coatings ensures a continuous supply of WS_2 layers at the contact interface in order to ensure a stable and low friction even after 2400 s of running. In Fig. 9, which shows the wear tracks after 2400 s of tribological testing, a continuous tribofilm can still be observed on both substrate and counterbody spray coated with WS_2. Raman confirms these findings, showing again a spectrum containing WS_2/WO_3 characteristic peaks. In comparison with the short term tests the intensity of the peaks corresponding to WO_3 increases in relation to WS_2, indicating tribochemical oxidation of the solid lubricant particles. According to [51], oxidation of 2D WS_2 nanosheets into a WS_2/WO_3 heterostructure starts at 350 °C upon exposure to oxidising atmosphere, a temperature which might be well reached at the asperities during continuous sliding. This mild degradation of the coating explains why the COF is slightly increasing towards the end of the long-term experiment. This is in good agreement with an earlier study, showing that the ratio between WO_3 and WS_2 increases for higher number of sliding cycles, being a clear indicator of coating failure [52]. In contrast, the sample spray coated with Bi_2S_3 shows high wear, similar to the reference surface after 900 s of testing. Furthermore, no peaks related to Bi_2S_3 can be found in the Raman spectrum, whereas peaks of Fe_3O_4 can be clearly identified. This explains the COFs at the end of the long term experiments with Bi_2S_3 at room temperature, and indicate a fast transition to high wear once the coating fails.

For the measurements performed at 100 °C with the uncoated reference and the plasma sprayed samples, the wear behaviour is almost identical to the one observed at room temperature (Fig. 10). All three systems show severe wear and Raman demonstrates severe tribooxidation of the substrate for all systems. This is clear evidence of coating failure and subsequent high friction and wear.

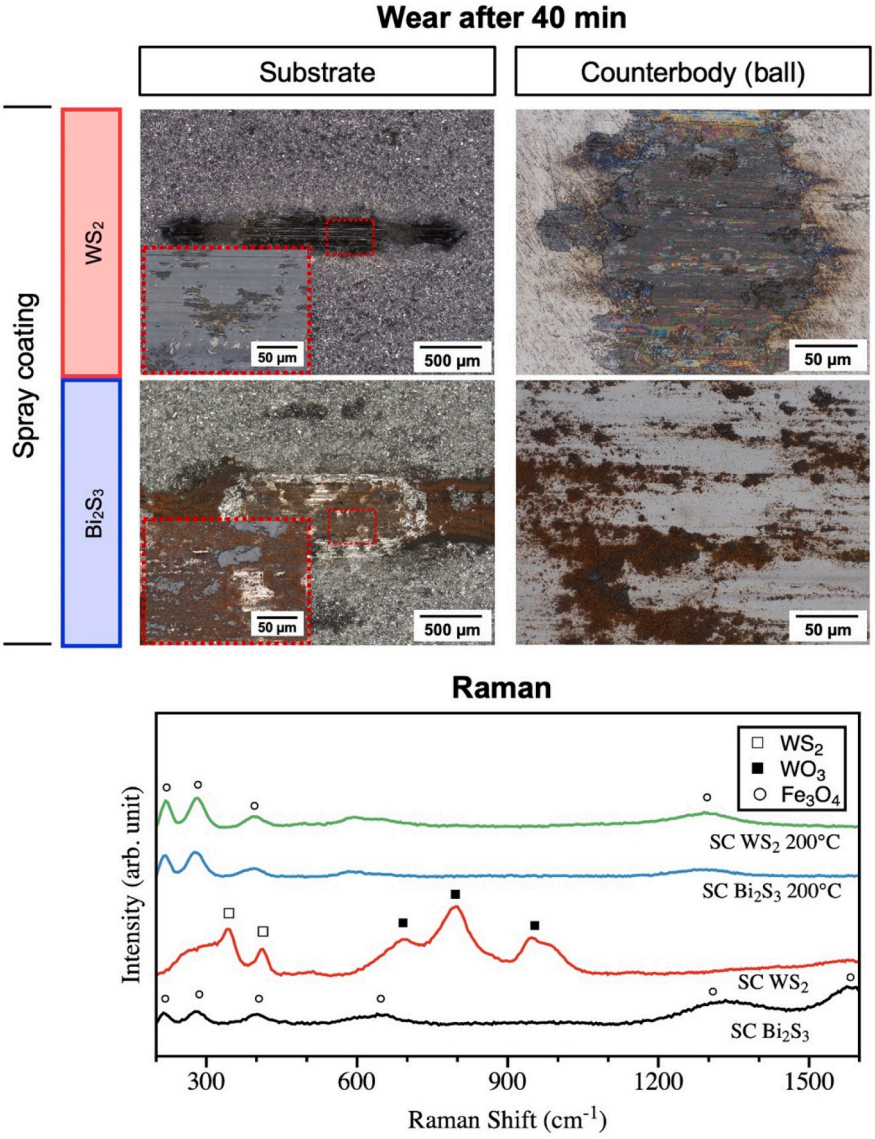

Fig. 9. Light microscopy images of the wear tracks on the substrates (left) and counterbodies (right) tested at room temperature for 2400 s (40 min). The coatings were fabricated by spray coating with WS_2 and Bi_2S_3 particles. Magnified views for individual wear track positions are shown for the regions highlighted by red rectangles. Below, Raman spectra taken within the wear tracks on the WS_2 and Bi_2S_3 spray coated substrates measured at room temperature and at 200 °C are shown.

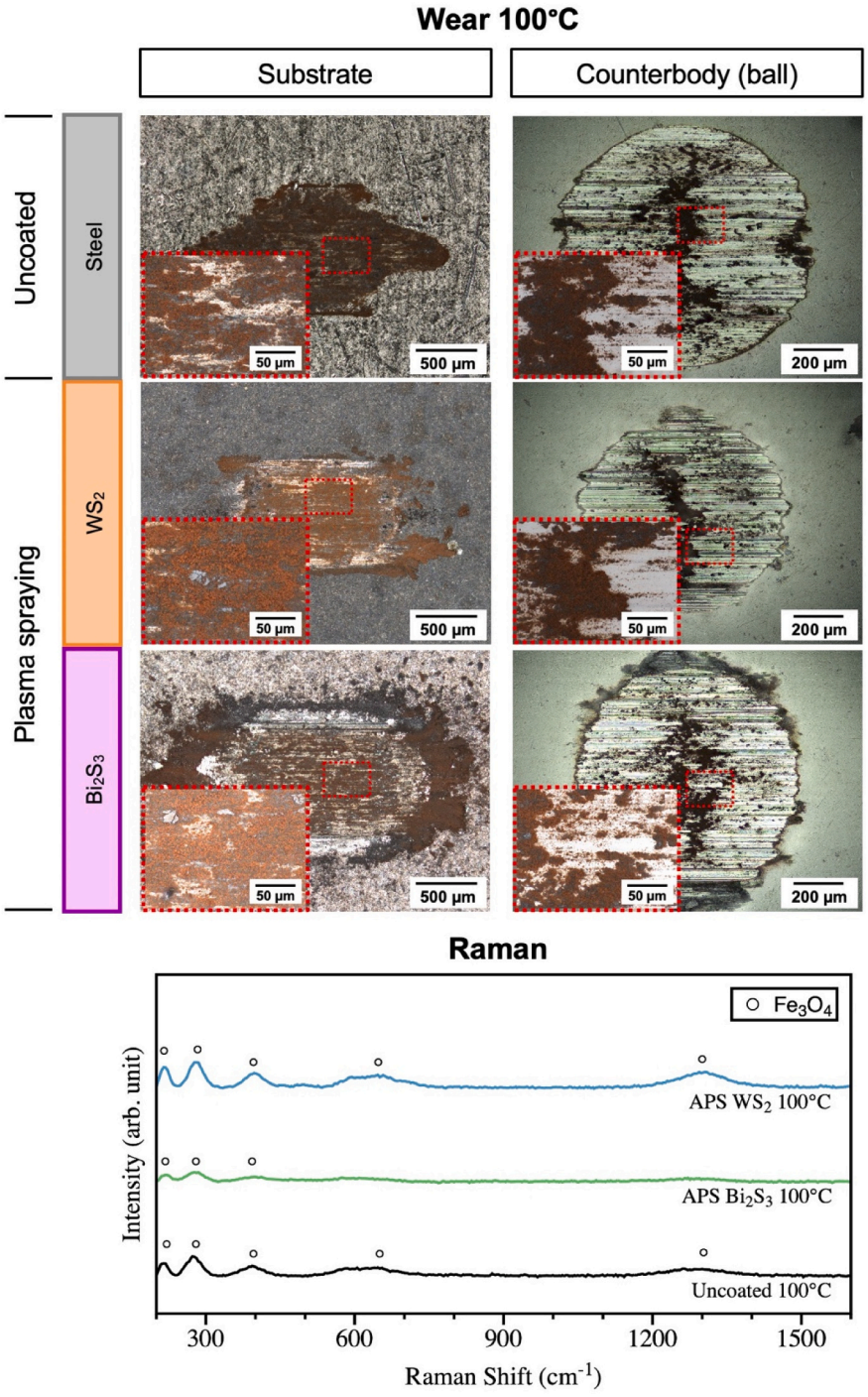

Fig. 10. Light microscopy images of the wear tracks on the substrates (left) and counterbodies (right) tested at 100 °C for the uncoated reference sample as well as the systems fabricated by plasma spraying with WS_2 and Bi_2S_3 particles. Magnified views for individual wear track positions are shown for the regions highlighted by red rectangles. Below, Raman spectra taken within the wear tracks on the WS_2 and Bi_2S_3 plasma sprayed substrates measured at 100 °C are shown.

The wear morphology of the reference and spray coated systems after the measurements at 200 °C for 900 s is in good agreement with the presented friction results (Fig. 11). The reference sample shows slightly higher wear, which might be associated with the stronger oxidation of the steel and the formation of a higher number of abrasive oxidic wear debris. The spray coated WS_2 sample on the other hand still shows negligible wear on the substrate after 900 s of sliding at 200 °C, demonstrating that the protective function of the tribofilm is still intact and low friction can prevail due to low shear between individual WS_2 layers. Evidence of this are the Raman measurements, which still show strong peaks corresponding to WS_2 and WO_3. However, several factors indicate an imminent failure of the coating. Firstly, the thickness of the tribofilm on the substrate is substantially reduced, as demonstrated by the clear appearance of the substrate underneath the tribofilm. Secondly, there is higher wear of the counterbody. Finally, Raman shows also an emerging Fe_3O_4 peak, also indicating incipient oxidative wear. Since it has been shown that oxidation of WS_2 nanosheets starts at 350 °C it can be an indication that this temperature is reached much faster when testing at an initial temperature of 200 °C. The oxidation process of the solid lubricant leads to the formation of non-lubricious

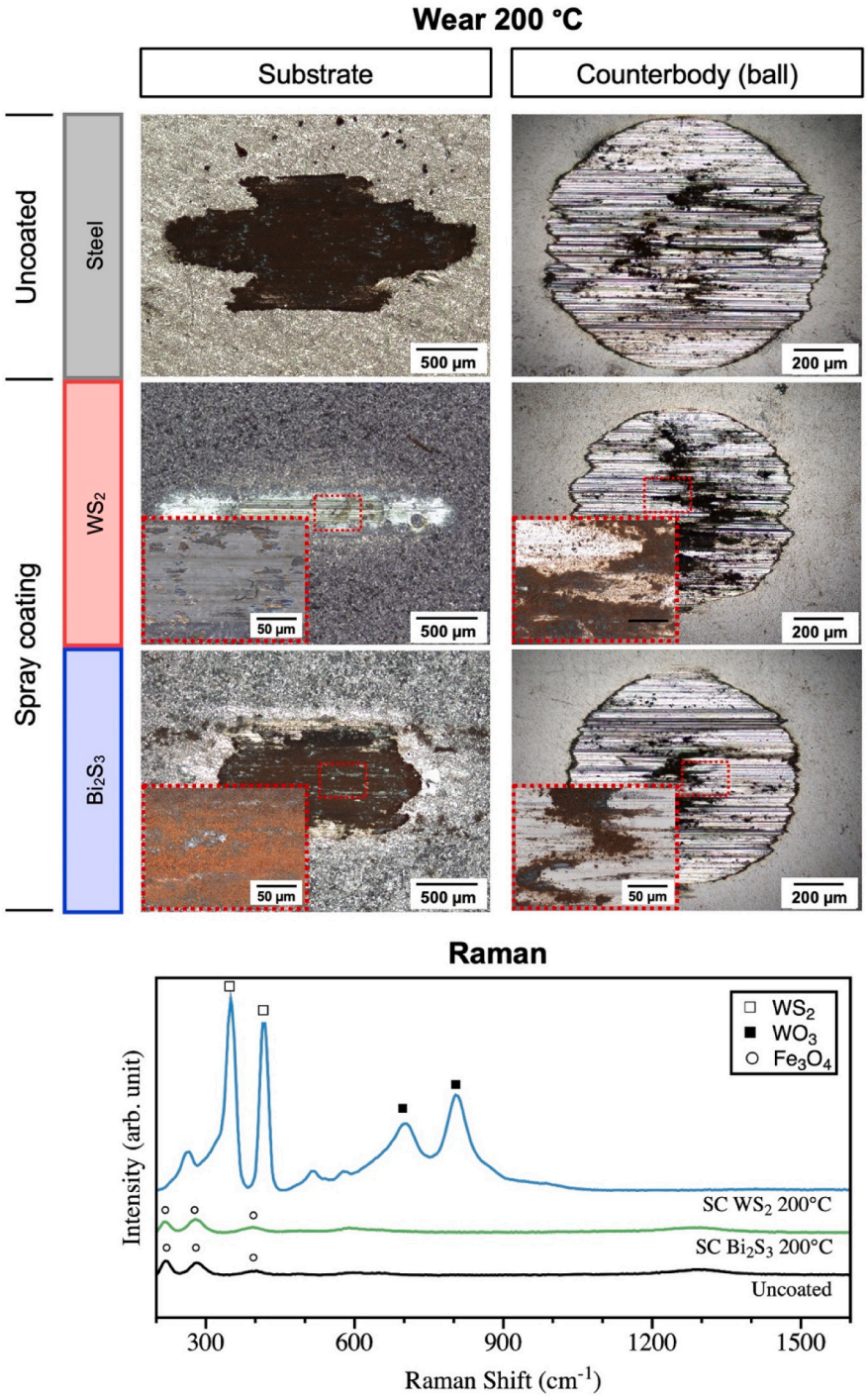

Fig. 11. Light microscopy images of the wear tracks on the substrates (left) and counterbodies (right) tested at 200 °C for the uncoated reference sample as well as the systems fabricated by spray coating with WS_2 and Bi_2S_3 particles. Magnified views for individual wear track positions are shown for the regions highlighted by red rectangles. Below, Raman spectra taken within the wear tracks on the WS_2 and Bi_2S_3 spray coated substrates measured at 200 °C are shown.

and abrasive WO_3, which results in a faster removal of the tribofilm and ultimately to failure of the coating. This is demonstrated by the increase in friction for the long term measurement of the sample spray coated with WS_2 (Fig. 7) and verified by the Raman measurements merely showing iron oxides (Fig. 9). Faster failure of the coating when measured at 200 °C is also observed for the spray coated Bi_2S_3 sample. At this temperature high wear, complete removal of the coating, and oxidation of the underlying surfaces are observed already after 900 s of testing, which verifies the failure of the Bi_2S_3 spray coating at this temperature.

4. Conclusions

The present work has investigated the influence of the deposition technique on the tribological properties of WS_2 and Bi_2S_3 low friction coatings. The results show that the use of atmospheric plasma spraying as coating technique results in the deposition of dense coatings with an excellent binding to the substrate. However, thermal degradation of WS_2 and Bi_2S_3 mainly into metallic W and Bi during deposition results in a substantial deterioration of their tribological properties. In contrast, when using spray coating the chemical composition and layered

morphology of the feedstock powders were maintained during the deposition process. This resulted in coatings demonstrating low friction and wear, even though at a lower coating density compared to plasma spray depositions.

While we observed low and stable steady-state friction at room temperature for both WS_2 and Bi_2S_3 deposited by spray coating, the performance of WS_2 is with a steady-state COF of 0.13 slightly superior to Bi_2S_3 (COF = 0.20). Additionally, the WS_2 coatings had an improved lifetime compared to Bi_2S_3. These tendencies are even more obvious at 200 °C, where WS_2 had a coefficient of friction of 0.15 versus 0.4 for Bi_2S_3 and longer lifetime. However, increasing the sample temperature results in a higher ratio of WO_3 to WS_2 with a subsequent shorter lifetime of the coating. These results emphasize the applicability of WS_2 from room temperature to at least 200 °C, a temperature already beyond the operational range of some conventional lubricants. On the other hand, the use of Bi_2S_3 coatings could be an alternative for less demanding applications.

CRediT authorship contribution statement

Philipp G. Grützmacher: Conceptualization, Methodology, Writing - Original Draft, Visualization, Supervision Michael Schranz: Investigation, Writing - Review & Editing, Visualization Chia-Jui Hsu: Investigation, Visualization Johannes Bernardi: Investigation Andreas Steiger-Thirsfeld: Investigation Lars Hensgen: Conceptualization, Visualization Manel Rodríguez Ripoll: Investigation, Writing - Review & Editing Carsten Gachot: Conceptualization, Writing - Review & Editing, Supervision, Project administration.

Declaration of competing interest

The authors declare that they have no known competing financial interests or personal relationships that could have appeared to influence the work reported in this paper.

Data availability

Data will be made available on request.

Acknowledgements

This work was funded by the Austrian COMET Programme (Project K2 InTribology, Grant No. 872176) and has been carried out within the "Austrian Excellence Center for Tribology" (AC2T research GmbH). Sebastian Spalt (INOCON Technologie GmbH) is kindly acknowledged for performing the coating depositions by atmospheric plasma spraying. Lukas Spiller (AC2T research GmbH) is kindly acknowledged for performing the tribological experiments. The authors acknowledge TU Wien Bibliothek for financial support through its Open Access Funding Programme.

References

[1] T.W. Scharf, S.V. Prasad, Solid lubricants: a review, J. Mater. Sci. 48 (2013) 511–531, https://doi.org/10.1007/s10853-012-7038-2.
[2] P. Gonzalez-Rodriguez, K.J.H. Van Den Nieuwenhuijzen, W. Lette, D.J. Schipper, J. E. Ten Elshof, Tribochemistry of bismuth and bismuth salts for solid lubrication, ACS Appl. Mater. Interfaces 8 (2016) 7601–7606, https://doi.org/10.1021/acsami.6b02541.
[3] A. Rosenkranz, H.L. Costa, M.Z. Baykara, A. Martini, Synergetic effects of surface texturing and solid lubricants to tailor friction and wear – a review, Tribol. Int. 155 (2021), 106792, https://doi.org/10.1016/j.triboint.2020.106792.
[4] T.W. Scharf, S.V. Prasad, Solid lubricants: a review, J. Mater. Sci. 48 (2013) 511–531, https://doi.org/10.1007/s10853-012-7038-2.
[5] H. Torres, M. Rodríguez Ripoll, B. Prakash, Tribological behaviour of self-lubricating materials at high temperatures, Int. Mater. Rev. 63 (2018) 309–340, https://doi.org/10.1080/09506608.2017.1410944.
[6] W.A. Brainard, in: The Thermal Stability And Friction of the Disulfides, Diselenides, And Ditellurides of Molybdenum And Tungsten in Vacuum (10-9 to 10-6 TORR), NASA Technical Note D-5141, 1968, pp. 1–26.
[7] K.S. Novoselov, A.K. Geim, S.V. Morozov, D. Jiang, Y. Zhang, S.V. Dubonos, I. V. Grigorieva, A.A. Firsov, Electric field effect in atomically thin carbon films, Science 306 (2004) 666–669, https://doi.org/10.1126/science.1102896.
[8] D. Berman, A. Erdemir, A.V. Sumant, Graphene: a new emerging lubricant, Mater. Today 17 (2014) 31–42, https://doi.org/10.1016/j.mattod.2013.12.003.
[9] C. Lee, X. Wei, Q. Li, R. Carpick, J.W. Kysar, J. Hone, Elastic and frictional properties of graphene, Phys. Status Solidi B 246 (2009) 2562–2567, https://doi.org/10.1002/pssb.200982329.
[10] W. Wang, G. Xie, J. Luo, Superlubricity of black phosphorus as lubricant additive, ACS Appl. Mater. Interfaces 10 (2018) 43203–43210, https://doi.org/10.1021/acsami.8b14730.
[11] C. Lee, Q. Li, W. Kalb, X.Z. Liu, H. Berger, R.W. Carpick, J. Hone, Frictional characteristics of atomically thin sheets, Science 328 (2010) 76–80, https://doi.org/10.1126/science.1184167.
[12] P.G. Grützmacher, S. Suarez, A. Tolosa, C. Gachot, G. Song, B. Wang, V. Presser, F. Mücklich, B. Anasori, A. Rosenkranz, Superior wear-resistance of Ti3C2Tx multilayer coatings, ACS Nano 15 (2021) 8216–8224, https://doi.org/10.1021/acsnano.1c01555.
[13] A. Rosenkranz, P.G. Grützmacher, R. Espinoza, V.M. Fuenzalida, E. Blanco, N. Escalona, F.J. Gracia, R. Villarroel, L. Guo, R. Kang, F. Mücklich, S. Suarez, Z. Zhang, Multi-layer Ti3C2Tx-nanoparticles (MXenes) as solid lubricants – role of surface terminations and intercalated water, Appl. Surf. Sci. 494 (2019) 13–21, https://doi.org/10.1016/j.apsusc.2019.07.171.
[14] P.C. Uzoma, H. Hu, M. Khadem, O.V. Penkov, Tribology of 2D nanomaterials: a review, Coatings 10 (2020), https://doi.org/10.3390/COATINGS10090897.
[15] M.Z. Baykara, M.R. Vazirisereshk, A. Martini, Emerging superlubricity: a review of the state of the art and perspectives on future research, <sb:contribution><sb:title>Appl. </sb:title></sb:contribution><sb:host><sb:issue><sb:series><sb:title>Phys. Rev.</sb:title></sb:series></sb:issue></sb:host> 5 (2018) 1–18, https://doi.org/10.1063/1.5051445.
[16] M.R. Vazirisereshk, A. Martini, D.A. Strubbe, M.Z. Baykara, Solid lubrication with MoS2: a review, Lubricants 7 (2019), https://doi.org/10.3390/LUBRICANTS7070057.
[17] P.C. Uzoma, H. Hu, M. Khadem, O.V. Penkov, Tribology of 2D nanomaterials: a review, Coatings 10 (2020), https://doi.org/10.3390/COATINGS10090897.
[18] P. Gonzalez-Rodriguez, K.J.H. Van Den Nieuwenhuijzen, W. Lette, D.J. Schipper, J. E. Ten Elshof, Tribochemistry of bismuth and bismuth salts for solid lubrication, ACS Appl. Mater. Interfaces 8 (2016) 7601–7606, https://doi.org/10.1021/acsami.6b02541.
[19] V. An, Y. Irtegov, C. De Izarra, Study of tribological properties of nanolamellar WS2 and MoS2 as additives to lubricants, J. Nanomater. 2014 (2014), https://doi.org/10.1155/2014/865839.
[20] S. Zhang, T. Ma, A. Erdemir, Q. Li, Tribology of two-dimensional materials: from mechanisms to modulating strategies, Mater. Today 26 (2019) 67–86, https://doi.org/10.1016/j.mattod.2018.12.002.
[21] C. Donnet, A. Erdemir, Solid lubricant coatings: recent developments and future trends, Tribol. Lett. 17 (2004) 389–397, https://doi.org/10.1023/B:TRIL.0000044487.32514.1d.
[22] M. Marian, D. Berman, A. Rota, R.L. Jackson, A. Rosenkranz, Layered 2D nanomaterials to tailor friction and wear in machine elements—a review, <sb:contribution><sb:title>Adv. Mater.</sb:title></sb:contribution><sb:host><sb:issue><sb:series><sb:title>Interfaces</sb:title></sb:series></sb:issue></sb:host> 2101622 (2021) 1–19, https://doi.org/10.1002/admi.202101622.
[23] A. Rosenkranz, P.G. Grützmacher, R. Espinoza, V.M. Fuenzalida, E. Blanco, N. Escalona, F.J. Gracia, R. Villarroel, L. Guo, R. Kang, F. Mücklich, S. Suarez, Z. Zhang, Multi-layer Ti3C2Tx-nanoparticles (MXenes) as solid lubricants – role of surface terminations and intercalated water, Appl. Surf. Sci. 494 (2019) 13–21, https://doi.org/10.1016/j.apsusc.2019.07.171.
[24] D. Berman, A. Erdemir, A.V. Sumant, Few layer graphene to reduce wear and friction on sliding steel surfaces, Carbon 54 (2013) 454–459, https://doi.org/10.1016/j.carbon.2012.11.061.
[25] A. Shirani, T. Joy, A. Rogov, M. Lin, A. Yerokhin, J.E. Mogonye, A. Korenyi-Both, S. M. Aouadi, A.A. Voevodin, D. Berman, PEO-chameleon as a potential protective coating on cast aluminum alloys for high-temperature applications, Surf. Coat. Technol. 397 (2020), 126016, https://doi.org/10.1016/j.surfcoat.2020.126016.
[26] S.M. Gateman, S.A. Alidokht, E. Mena-Morcillo, R. Schulz, R.R. Chromik, A. M. Kietzig, I.P. Parkin, J. Mauzeroll, Wear resistant solid lubricating coatings via compression molding and thermal spraying technologies, Surf. Coat. Technol. 426 (2021), 127790, https://doi.org/10.1016/j.surfcoat.2021.127790.
[27] L. Reinert, F. Lasserre, C. Gachot, P.G. Grützmacher, T. Maclucas, N. Souza, F. Mücklich, S. Suarez, Long-lasting solid lubrication by CNT-coated patterned surfaces, Sci. Rep. 7 (2017) 42873, https://doi.org/10.1038/srep42873.
[28] C. Muratore, A.A. Voevodin, N.R. Glavin, Physical vapor deposition of 2D Van der Waals materials: a review, Thin Solid Films 688 (2019), 137500, https://doi.org/10.1016/j.tsf.2019.137500.
[29] X. Wang, Y. Zhang, Z. Yin, Frequent start-stop test study of Graphene coatings on journal bearings, in: Key Engineering Materials 841 KEM, 2020, pp. 26–35, https://doi.org/10.4028/www.scientific.net/KEM.841.26.
[30] T.W. Scharf, D.R. Diercks, B.P. Gorman, S.V. Prasad, M.T. Dugger, Atomic layer deposition of tungsten disulphide solid lubricant nanocomposite coatings on rolling element bearings, Tribol. Trans. 52 (2009) 284–292, https://doi.org/10.1080/10402000802369747.
[31] M. Marian, D. Berman, A. Rota, R.L. Jackson, A. Rosenkranz, Layered 2D nanomaterials to tailor friction and wear in machine elements—a review, <sb:

contribution><sb:title>Adv. Mater.</sb:title></sb:contribution><sb:host><sb:issue><sb:series><sb:title>Interfaces</sb:title></sb:series></sb:issue></sb:host> 2101622 (2021) 1–19, https://doi.org/10.1002/admi.202101622.
[32] H. Herman, S. Sampath, R. McCune, Thermal spray: current status and future trends, MRS Bull. 25 (2000) 17–25, https://doi.org/10.1557/mrs2000.119.
[33] S.M. Gateman, S.A. Alidokht, E. Mena-Morcillo, R. Schulz, R.R. Chromik, A. M. Kietzig, I.P. Parkin, J. Mauzeroll, Wear resistant solid lubricating coatings via compression molding and thermal spraying technologies, Surf. Coat. Technol. 426 (2021), 127790, https://doi.org/10.1016/j.surfcoat.2021.127790.
[34] H. Chen, Y. Zhang, C. Ding, Tribological properties of nanostructured zirconia coatings deposited by plasma spraying, Wear 253 (2002) 885–893, https://doi.org/10.1016/S0043-1648(02)00221-1.
[35] H. Herman, S. Sampath, R. McCune, Thermal spray: current status and future trends, MRS Bull. 25 (2000) 17–25, https://doi.org/10.1557/mrs2000.119.
[36] A.V. Ayyagari, K.C. Mutyala, A.V. Sumant, Towards developing robust solid lubricant operable in multifarious environments, Sci. Rep. 10 (2020) 1–12, https://doi.org/10.1038/s41598-020-72666-4.
[37] D. Garcia-Alonso, N. Serres, C. Demian, S. Costil, C. Langlade, C. Coddet, Pre-/during-/post-laser processes to enhance the adhesion and mechanical properties of thermal-sprayed coatings with a reduced environmental impact, J. Therm. Spray Technol. 20 (2011) 719–735, https://doi.org/10.1007/s11666-011-9629-x.
[38] P.J. Blau, On the nature of running-in, Tribol. Int. 38 (2005) 1007–1012, https://doi.org/10.1016/j.triboint.2005.07.020.
[39] B. Kohlhauser, M.R. Ripoll, H. Riedl, C.M. Koller, N. Koutna, A. Amsüss, H. Hutter, G. Ramirez, C. Gachot, A. Erdemir, P.H. Mayrhofer, How to get noWear? – a new take on the design of in-situ formed high performing low-friction tribofilms, Mater. Des. 190 (2020), 108519, https://doi.org/10.1016/j.matdes.2020.108519.
[40] A.R. Lansdown, High-temperature lubrication, Proc. Inst. Mech. Eng. C Mech. Eng. Sci. 204 (1990) 279–291, https://doi.org/10.1243/PIME_PROC_1990_204_109_02.
[41] I. Velkavrh, F. Autserer, S. Klien, J. Voyer, A. Ristow, J. Brenner, P. Forêt, A. Diem, The influence of temperature on friction and wear of unlubricated steel/steel contacts in different gaseous atmospheres, Tribol. Int. 98 (2016) 155–171, https://doi.org/10.1016/j.triboint.2016.02.022.
[42] F.H. Stott, High-temperature sliding wear of metals, Tribol. Int. 35 (2002) 489–495, https://doi.org/10.1016/S0301-679X(02)00041-5.
[43] Z. Jiang, Y. Zhang, G. Yang, K. Yang, S. Zhang, L. Yu, P. Zhang, Tribological properties of oleylamine-modified ultrathin WS2 nanosheets as the additive in polyalpha olefin over a wide temperature range, Tribol. Lett. 61 (2016) 1–14, https://doi.org/10.1007/s11249-016-0643-5.
[44] B. Pilotti, G. Prieto, A. Juan, R. Faccio, E. Broitman, M. Dennehy, W.R. Tuckart, Bi2S3 and MoS2 soft coatings: a comparative study of their frictional behavior under different humidity levels, Normal loads, and sliding speeds, Tribol. Lett. 69 (2021), https://doi.org/10.1007/s11249-021-01486-y.
[45] Y. Li, H. Lu, Q. Liu, L. Qin, G. Dong, A facile method to enhance the tribological performances of MoSe2 nanoparticles as oil additives, Tribol. Int. 137 (2019) 22–29, https://doi.org/10.1016/j.triboint.2019.04.029.
[46] D.L.A. de Faria, S. Venâncio Silva, M.T. de Oliveira, Raman microspectroscopy of some iron oxides and oxyhydroxides, J. Raman Spectrosc. 28 (2002) 873–878, https://doi.org/10.1002/(sici)1097-4555(199711)28:11<873::aid-jrs177>3.3.co;2-2.
[47] T. Suszko, W. Gulbiński, J. Jagielski, The role of surface oxidation in friction processes on molybdenum nitride thin films, Surf. Coat. Technol. 194 (2005) 319–324, https://doi.org/10.1016/j.surfcoat.2004.07.119.
[48] A. Berkdemir, H.R. Gutiérrez, A.R. Botello-Méndez, N. Perea-López, A.L. Elías, C. I. Chia, B. Wang, V.H. Crespi, F. López-Urías, J.C. Charlier, H. Terrones, M. Terrones, Identification of individual and few layers of WS2 using Raman spectroscopy, Sci. Rep. 3 (2013) 1–8, https://doi.org/10.1038/srep01755.
[49] M. Boulova, G. Lucazeau, Crystallite nanosize effect on the structural transitions of WO3 studied by Raman spectroscopy, J. Solid State Chem. 167 (2002) 425–434, https://doi.org/10.1006/jssc.2002.9649.
[50] I. Zumeta-Dubé, J.L. Ortiz-Quiñonez, D. Díaz, C. Trallero-Giner, V.F. Ruiz-Ruiz, First order Raman scattering in bulk Bi2S3 and quantum dots: reconsidering controversial interpretations, J. Phys. Chem. C 118 (2014) 30244–30252, https://doi.org/10.1021/jp509636n.
[51] H.K. Adigilli, B. Padya, L. Venkatesh, V.S.K. Chakravadhanula, A.K. Pandey, J. Joardar, Oxidation of 2D-WS2 nanosheets for generation of 2D-WS2/WO3 heterostructure and 2D and nanospherical WO3, Phys. Chem. Chem. Phys. 21 (2019) 25139–25147, https://doi.org/10.1039/c9cp01890e.
[52] M.R. Ripoll, R. Simic, J. Brenner, B. Podgornik, Friction and lifetime of laser surface-textured and MoS2-coated Ti 6Al4V under dry reciprocating sliding, Tribol. Lett. 51 (2013) 261–271, https://doi.org/10.1007/s11249-013-0170-6.